Advances in Applied Mathematics and Mechanics
Adv. Appl. Math. Mech., Vol. **8**, No. 3, pp. 449-463

DOI: 10.4208/aamm.2014.m600
June 2016

Study of Heat Transfer Control with Magnetic Field Using Higher Order Finite Difference Scheme

R. Sivakumar[1], S. Vimala[2], S. Damodaran[3] and T. V. S. Sekhar[4,*]

[1] *Department of Physics, Pondicherry University, Puducherry-605 014, India*
[2] *Department of Mathematics, Pondicherry Engineering College, Puducherry-605 014, India*
[3] *Department of Mathematics, Bharathidasan Govt. College for Women, Puducherry-605 003, India*
[4] *School of Basic Sciences, Indian Institute of Technology Bhubaneswar, Bhubaneswar-751 007, India*

Received 10 November 2014; Accepted (in revised version) 17 March 2015

Abstract. The control of convective heat transfer from a heated circular cylinder immersed in an electrically conducting fluid is achieved using an externally imposed magnetic field. A Higher Order Compact Scheme (HOCS) is used to solve the governing energy equation in cylindrical polar coordinates. The HOCS gives fourth order accurate results for the temperature field. The behavior of local Nusselt number, mean Nusselt number and temperature field due to variation in the aligned magnetic field is evaluated for the parameters $5 \leq Re \leq 40$, $0 \leq N \leq 20$ and $0.065 \leq Pr \leq 7$. It is found that the convective heat transfer is suppressed by increasing the strength of the imposed magnetic field until a critical value of N, the interaction parameter, beyond which the heat transfer increases with further increase in N. The results are found to be in good agreement with recent experimental studies.

AMS subject classifications: 76D05, 65N06

Key words: Higher Order Compact Scheme, forced convection, magnetic field, low R_m approximation.

1 Introduction

Magnetic fields are now being employed in control of fluids and in metallurgical processing where liquid metals are involved. The principal effect in action being the Lorentz force produced in the electrically conducting fluid in magnetic field. Further, the magnetic field is useful to eliminate unwanted recirculation bubble or turbulent motion of fluid.

*Corresponding author.
Email: rsk.phy@pondiuni.edu.in (R. Sivakumar), vimalaks@pec.edu (S. Vimala), sreedamo@gmail.com (S. Damodaran), sekhartvs@iitbbs.ac.in (T. V. S. Sekhar)

 ©2016 Global Science Press

https://doi.org/10.4208/aamm.2014.m600 Published online by Cambridge University Press

When an electrically conducting fluid moves in presence of a uniform external magnetic field, electric current is produced in the fluid, which slowly dissipates in the fluid in the form of heat energy via Ohm's law. The dissipation of heat energy in the moving fluid causes considerable modification in the thermal convection and fluid flow structure. In particular it is known that rate of fluid flow gets damped due to the imposed uniform magnetic field. Hence it is of particular interest to investigate the nature of heat transfer in the presence of MHD effects [1]. Fluid flow control using magnetic field is based on a solid physical foundation. This has scope for technology that aids in a better heat transfer control. Applications like fusion technology have made hydromagnetic flows of electrically conducting fluid and their heat transfer more important in recent years. The study of magnetic heat transfer over a sphere has been explored experimentally by Boynton [2]. Uda et al. [3] experimentally studied MHD effects on heat transfer of liquid Lithium flow in an annular channel. Yokomine et al. [4] investigated heat transfer properties of aqueous KOH solution ($Pr \approx 5$) in their experimental study and concluded that there is a degradation of heat transfer with magnetic field. The electromagnetic enhancement of heat transfer has also been found [5]. The heat transfer from the side-wall of a duct through which an electrically conducting fluid flows within a strong transverse magnetic field [6] and the heat transfer around a circular cylinder placed in a rectangular channel subject to the externally applied magnetic field [7] have been investigated in recent times. The magnetic effect on forced convection around a circular cylinder embedded in a porus medium has also been investigated [8]. An experimental study [9] provided the evidence that an externally applied magnetic field can help to suppress vortex shedding. In this regard, numerical studies have been conducted later to understand the flow instability that is present in the wake using magnetic fields and it was found that depending on the magnitude of applied magnetic fields in the two-dimensional flow region, the vortex shedding can be suppressed or eliminated and as a result the flow becomes stabilized [10–12].

Higher Order Compact Schemes (HOCS) are becoming more popular in recent days due to their higher order of accuracy in results in addition to unconditional stability of the numerical scheme. These schemes capture the flow phenomena very accurately in coarser grids itself when compared to upwind schemes and also some second order accurate finite difference schemes [13–15]. In this paper, control of heat transfer from a heated circular cylinder immersed in a steady stream of viscous incompressible and electrically conducting fluid which is under the influence of an externally imposed magnetic field is studied using higher order finite difference scheme. The behavior of local and mean Nusselt numbers is then compared with recent experimental results.

2 Formulation of the problem

The forced convective heat transfer problem is formulated as steady, laminar flow in axissymmetric cylindrical polar coordinates. The center of the cylinder is chosen at origin

https://doi.org/10.4208/aamm.2014.m600 Published online by Cambridge University Press

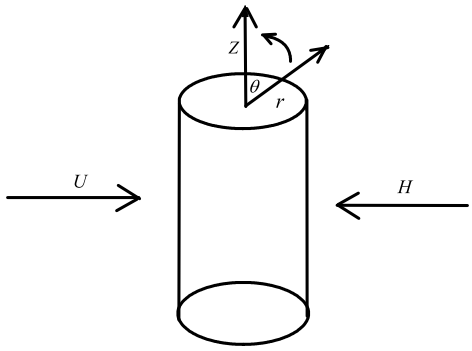


Figure 1: Schematic representation of the flow configuration.

and the flow is symmetric about $\theta=\pi$ (upstream) and $\theta=0^\circ$ (downstream). The fluid is considered to be incompressible viscous and electrically conducting. An uniform stream from infinity, U_∞ is imposed from left to right at far distances from the cylinder. The magnetic Reynolds number is assumed to be small so that induced magnetic field can be neglected (low R_m approximation) and a constant magnetic field [16, 17]

$$\mathbf{H}=(-\cos\theta,\sin\theta,0) \tag{2.1}$$

is imposed opposite to the flow. A schematic diagram showing the flow configuration is depicted in Fig. 1. The flow is described by Navier-Stokes equations and Maxwell's equations.

$$(\mathbf{u}\cdot\boldsymbol{\nabla})\mathbf{u}=-\boldsymbol{\nabla}p+\frac{2}{Re}\nabla^2\mathbf{u}+N[(\mathbf{u}\times\mathbf{H})\times\mathbf{H}], \tag{2.2a}$$

$$\boldsymbol{\nabla}\cdot\mathbf{u}=\mathbf{0}, \tag{2.2b}$$

$$\boldsymbol{\nabla}\cdot\mathbf{H}=\mathbf{0}, \tag{2.2c}$$

$$\boldsymbol{\nabla}\times\boldsymbol{E}=\mathbf{0}, \tag{2.2d}$$

where p is the pressure, $\mathbf{u}$ the fluid velocity, $\mathbf{H}$ the magnetic field, $\mathbf{E}$ the electric field. While non-dimensionalizing the above equations, the length scale is taken as the radius of the cylinder a and the non-dimensional parameters evolved are the kinematic Reynolds number is $Re=2aU/\nu$ and the interaction parameter $N=\sigma H_\infty^2 a/\rho U_\infty$. The kinematic viscosity, density, magnetic permeability and electrical conductivity of the fluid are ν, ρ, μ and σ, respectively. By taking curl of the momentum equation (2.2), we get

$$-\boldsymbol{\nabla}\times(\boldsymbol{\nabla}\times\boldsymbol{\omega})=\frac{Re}{2}\boldsymbol{\nabla}\times(\boldsymbol{\omega}\times\mathbf{u})-\frac{ReN}{2}\boldsymbol{\nabla}\times\{(\mathbf{u}\times\mathbf{H})\times\mathbf{H}\}, \tag{2.3a}$$

$$\boldsymbol{\omega}=\boldsymbol{\nabla}\times\mathbf{u}, \tag{2.3b}$$

where $\boldsymbol{\omega}$ is the vorticity. Since the flow is two dimensional, $\mathbf{E}=\mathbf{0}$. Cylindrical polar co-ordinates (r,θ,z) are used as they are most suitable in dealing with cylindrical boundaries.

https://doi.org/10.4208/aamm.2014.m600 Published online by Cambridge University Press

The co-ordinate system is set up such that the velocity and magnetic field are parallel at large distances and the flow is symmetric about $\theta=0^\circ$ and $\theta=180^\circ$. Here, $\mathbf{u}=(u_r,u_\theta,0)$. These velocity components are expressed in terms of a dimensionless stream function $\psi(\xi,\theta)$ such that the equation of continuity $\boldsymbol{\nabla}\cdot\mathbf{u}=0$ is satisfied. They are

$$u_r=\frac{1}{r}\frac{\partial\psi}{\partial\theta},\quad u_\theta=-\frac{\partial\psi}{\partial r}. \tag{2.4}$$

We use the transformation $r=e^{\pi\xi}$ and $\theta=\pi\eta$ and consequently, the flow equations become

$$\frac{\partial^2\psi}{\partial\xi^2}+\frac{\partial^2\psi}{\partial\eta^2}+\pi^2e^{2\pi\xi}\omega=0, \tag{2.5a}$$

$$\begin{aligned}&\frac{\partial^2\omega}{\partial\xi^2}+\frac{\partial^2\omega}{\partial\eta^2}-\frac{Re}{2}\left[\frac{\partial\psi}{\partial\eta}\frac{\partial\omega}{\partial\xi}-\frac{\partial\psi}{\partial\xi}\frac{\partial\omega}{\partial\eta}\right]\\&=\frac{NRe}{2}\left[\pi^2e^{2\pi\xi}\omega\sin^2(\pi\eta)+\sin2(\pi\eta)\frac{\partial^2\psi}{\partial\xi\partial\eta}\right.\\&\qquad\left.-\pi\sin2(\pi\eta)\frac{\partial\psi}{\partial\eta}-\cos2(\pi\eta)\frac{\partial^2\psi}{\partial\xi^2}+\pi\cos2(\pi\eta)\frac{\partial\psi}{\partial\xi}\right].\end{aligned} \tag{2.5b}$$

Eqs. (2.5a) and (2.5b) must now be solved subject to the following boundary conditions. On the surface of the cylinder, no-slip condition is applied. At far off distances, uniform flow is imposed. The boundary conditions applied are (i) on the surface of the cylinder $\psi=\partial\psi/\partial\xi=0$ (ii) at large distances from cylinder $\psi\sim e^{\pi\xi}\sin(\pi\eta)$; and (iii) on the axis of symmetry $\psi=0$, $\omega=0$. The flow velocities are obtained by solving Eqs. (2.4) to (2.5b) using multigrid technique. More details of this technique and results are explained in Sekhar et al. [18]. Under the condition that the physical properties of the fluid are constant and the internal generation of heat by friction is neglected, the energy equation is given by

$$\mathbf{u}\cdot\boldsymbol{\nabla}T=\frac{2}{RePr}\nabla^2T. \tag{2.6}$$

In Cylindrical polar coordinates, using the given transformation, the energy equation is written as

$$\frac{\partial^2T}{\partial\xi^2}+\frac{\partial^2T}{\partial\eta^2}=\frac{RePr}{2}\left(\frac{\partial\psi}{\partial\eta}\frac{\partial T}{\partial\xi}-\frac{\partial\psi}{\partial\xi}\frac{\partial T}{\partial\eta}\right), \tag{2.7}$$

where $T(\xi,\eta)$ is the non-dimensionalized temperature, defined by subtracting the main-flow temperature T_∞ from the temperature and dividing by T_s-T_∞. The Prandtl number Pr is given by $Pr=\nu/\kappa$. The boundary conditions for temperature are (i) $T=1$ at $\xi=0$ on the surface of the cylinder, (ii) $T\to0$ as $\xi\to\infty$, at large distance from cylinder and (iii) along the axis of symmetry ($\eta=0$ and $\eta=1$); $\partial T/\partial\eta=0$.

3 Numerical method

The velocity field is obtained by solving Eqs. (2.4) to (2.5b) using a second order accurate finite difference based multigrid method followed by defect correction technique

https://doi.org/10.4208/aamm.2014.m600 Published online by Cambridge University Press

developed by Sekhar et al. [18]. The velocity obtained over a high resolution grid (say 512×512 or 1024×1024) is used to solve the energy equation. The fourth order accurate Higher Order Compact Scheme (HOCS) is used to solve the energy equation (2.7) as follows. Eq. (2.7) is rewritten as

$$-\frac{\partial^2 T}{\partial\xi^2}-\frac{\partial^2 T}{\partial\eta^2}+c\frac{\partial T}{\partial\xi}+d\frac{\partial T}{\partial\eta}=0, \tag{3.1}$$

where

$$c=\frac{RePr}{2}\pi e^{\pi\xi}u_r,\quad d=\frac{RePr}{2}\pi e^{\pi\xi}u_\theta. \tag{3.2}$$

The velocity components u_r and u_θ in the Eq. (3.2) are obtained using usual fourth order approximations from the stream function ψ. Applying standard central difference operators to Eq. (3.1) gives,

$$-\delta_\xi^2 T_{i,j}-\delta_\eta^2 T_{i,j}+c_{i,j}\delta_\xi T_{i,j}+d_{i,j}\delta_\eta T_{i,j}-\tau_{i,j}=0. \tag{3.3}$$

The truncation error of (3.3) is given by

$$\tau_{i,j}=\Big[2\Big(\frac{h^2}{12}c\frac{\partial^3 T}{\partial\xi^3}+\frac{k^2}{12}d\frac{\partial^3 T}{\partial\eta^3}\Big)-\Big(\frac{h^2}{12}\frac{\partial^4 T}{\partial\xi^4}+\frac{k^2}{12}\frac{\partial^4 T}{\partial\eta^4}\Big)\Big]_{i,j}+\mathcal{O}(h^4,k^4), \tag{3.4}$$

where h and k are grid spacing $(h\neq k)$ in the radial and angular directions, respectively.

From Eq. (2.7), we get

$$\begin{aligned}
\frac{\partial^3 T}{\partial\xi^3}&=-\frac{\partial^3 T}{\partial\xi\partial\eta^2}+c\frac{\partial^2 T}{\partial\xi^2}+\frac{\partial c}{\partial\xi}\frac{\partial T}{\partial\xi}+d\frac{\partial^2 T}{\partial\xi\partial\eta}+\frac{\partial d}{\partial\xi}\frac{\partial T}{\partial\eta},\\
\frac{\partial^4 T}{\partial\xi^4}&=-\frac{\partial^4 T}{\partial\xi^2\partial\eta^2}+d\frac{\partial^3 T}{\partial\xi^2\partial\eta}-c\frac{\partial^3 T}{\partial\xi\partial\eta^2}+\Big(2\frac{\partial d}{\partial\xi}+cd\Big)\frac{\partial^2 T}{\partial\xi\partial\eta}+\Big(2\frac{\partial c}{\partial\xi}+c^2\Big)\frac{\partial^2 T}{\partial\xi^2}\\
&\quad+\Big(\frac{\partial^2 c}{\partial\xi^2}+c\frac{\partial c}{\partial\xi}\Big)\frac{\partial T}{\partial\xi}+\Big(\frac{\partial^2 d}{\partial\xi^2}+c\frac{\partial d}{\partial\xi}\Big)\frac{\partial T}{\partial\eta},\\
\frac{\partial^3 T}{\partial\eta^3}&=-\frac{\partial^3 T}{\partial\xi^2\partial\eta}+c\frac{\partial^2 T}{\partial\xi\partial\eta}+\frac{\partial c}{\partial\eta}\frac{\partial T}{\partial\xi}+d\frac{\partial^2 T}{\partial\eta^2}+\frac{\partial d}{\partial\eta}\frac{\partial T}{\partial\eta},\\
\frac{\partial^4 T}{\partial\eta^4}&=-\frac{\partial^4 T}{\partial\xi^2\partial\eta^2}+c\frac{\partial^3 T}{\partial\xi\partial\eta^2}-d\frac{\partial^3 T}{\partial\xi^2\partial\eta}+\Big(2\frac{\partial c}{\partial\eta}+cd\Big)\frac{\partial^2 T}{\partial\xi\partial\eta}+\Big(2\frac{\partial d}{\partial\eta}+d^2\Big)\frac{\partial^2 T}{\partial\eta^2}\\
&\quad+\Big(\frac{\partial^2 c}{\partial\eta^2}+d\frac{\partial c}{\partial\eta}\Big)\frac{\partial T}{\partial\xi}+\Big(\frac{\partial^2 d}{\partial\eta^2}+d\frac{\partial d}{\partial\eta}\Big)\frac{\partial T}{\partial\eta}.
\end{aligned}$$

On substituting in Eq. (3.4) and using it in Eq. (3.3) gives

$$\begin{aligned}
&-e_{i,j}\delta_\xi^2 T_{i,j}-f_{i,j}\delta_\eta^2 T_{i,j}+g_{i,j}\delta_\xi T_{i,j}-o_{i,j}\delta_\eta T_{i,j}-D_2(\delta_\xi^2\delta_\eta^2 T_{i,j}-c_{i,j}\delta_\xi\delta_\eta^2 T_{i,j}-d_{i,j}\delta_\xi^2\delta_\eta T_{i,j})\\
&+w_{i,j}\delta_\eta\delta_\xi T_{i,j}=0,
\end{aligned}$$

https://doi.org/10.4208/aamm.2014.m600 Published online by Cambridge University Press

where the coefficients $e_{i,j}$, $f_{i,j}$, $g_{i,j}$, $o_{i,j}$ and $w_{i,j}$ are given by

$$e_{i,j}=1+\frac{h^2}{12}(c_{i,j}^2-2\delta_\xi c_{i,j}),\quad f_{i,j}=1+\frac{k^2}{12}(d_{i,j}^2-2\delta_\eta d_{i,j}),$$
$$g_{i,j}=c_{i,j}+\frac{h^2}{12}(\delta_\xi^2 c_{i,j}-c_{i,j}\delta_\xi c_{i,j})+\frac{k^2}{12}(\delta_\eta^2 c_{i,j}-d_{i,j}\delta_\eta c_{i,j}),$$
$$o_{i,j}=d_{i,j}+\frac{h^2}{12}(\delta_\xi^2 d_{i,j}-c_{i,j}\delta_\xi d_{i,j})+\frac{k^2}{12}(\delta_\eta^2 d_{i,j}-d_{i,j}\delta_\eta d_{i,j}),$$
$$w_{i,j}=\frac{h^2}{6}\delta_\xi d_{i,j}+\frac{k^2}{6}\delta_\eta c_{i,j}-D_2 c_{i,j}d_{i,j},$$

and

$$D_2=\frac{h^2+k^2}{12}.$$

The two-dimensional cross derivative δ operators such as $\delta_\xi\delta_\eta T_{i,j}$, $\delta_\xi^2\delta_\eta T_{i,j}$, $\delta_\xi\delta_\eta^2 T_{i,j}$, $\delta_\xi^2\delta_\eta^2 T_{i,j}$ for $h\neq k$ are approximated by the central differences.

While approximating the boundary conditions for temperature, $\partial T/\partial\eta$ is approximated by fourth order forward difference along $\eta=0$ and fourth order backward difference along $\eta=1$ as follows

$$T(i,1)=\frac{1}{25}\left[48T(i,2)-36T(i,3)+16T(i,4)-3T(i,5)\right],$$
$$T(i,m+1)=\frac{1}{25}\left[48T(i,m)-36T(i,m-1)+16T(i,m-2)-3T(i,m-3)\right].$$

The algebraic system of equations obtained using the fourth order compact scheme described as above are solved using Point Gauss-Seidel method. The scheme helps to achieve convergence up to 10^{-6} even at higher values of parameters

4 Results and discussion

A higher order compact scheme is applied to the problem of heated cylinder, which is immersed in an incompressible, viscous and electrically conducting fluid. The streamwise magnetic field is applied in the opposite direction of the flow to control the heat transfer. The flow results of Sekhar et al. [18] have been extended to higher values of N up to 20 using SYS-7047GR-TRF workstation and then forced convection is studied. In this study, the results are presented for two flows $Re=5$ (without flow separation), 40 (with flow separation) and N in the range $0\leq N\leq 20$. The heat flux $q(\theta)$ from the cylinder to the fluid is computed using

$$q(\theta)=\frac{k(T_s-T_\infty)}{a}\left(\frac{\partial T}{\partial\xi}\right)_{\xi=0}. \tag{4.1}$$

https://doi.org/10.4208/aamm.2014.m600 Published online by Cambridge University Press

The local Nusselt number $N_u(\theta)$ and the mean Nusselt number $\overline{Nu}$ are calculated as follows:

$$Nu(\theta) = \frac{2aq(\theta)}{k(T_s - T_\infty)} = \frac{-2}{\pi}\left(\frac{\partial T}{\partial \xi}\right)_{\xi=0}, \tag{4.2a}$$

$$\overline{Nu} = \frac{-2}{\pi}\int_0^1 \left(\frac{\partial T}{\partial \xi}\right)_{\xi=0} d\eta. \tag{4.2b}$$

In Eqs. (4.2a) and (4.2b) the derivative $\partial T/\partial \xi$ is approximated with fourth order finite differences.

4.1 Validation

In the absence of the magnetic field $(N=0)$ the basic hydrodynamic problem is equivalent to the steady viscous flow around a cylinder. Therefore, for $N=0$, the developed scheme is validated with the available theoretical results for different Re and Pr in Table 1. It is clear from the table that the present results agree well with the literature data [19, 20]. Fig. 2 shows the variation of drag coefficients with magnetic field while Fig. 3 displays the behavior of separation length and separation angle. The application of magnetic field increases the pressure and viscous drag coefficients. The non-monotonic variation of separation length and angle were explained using pressure field computation in our earlier work [18].

Table 1: Comparison of the mean Nusselt number with literature in the absence of the magnetic field.

Re	Pr	$\overline{Nu}$		
		Ref. [19]	Ref. [20]	Present
10	0.73	-	1.897	1.874
20	0.73	-	2.557	2.472
40	0.73	-	3.48	3.29
20	5	4.593	-	4.6

4.2 Local Nusselt number

The angular variation of the local Nusselt number Nu on the surface of the cylinder for different Prandtl numbers and interaction parameters are presented in Fig. 4. At $Re=40$, in the absence of the magnetic field, it is observed that the local Nusselt number decreases along the surface of the cylinder up to the point of separation and then increases. In the upstream region (Fig. 4), the viscous boundary layer thickens with the application of magnetic field. All the curves in this figure meet at one critical point after which an inverse effect is exhibited, that is, the boundary layer gets thinner with magnetic field. The curves meet once again in the far downstream. These features are attributed to changes in radial and transverse velocity gradients of the fluid which resulted due to the application of magnetic field to the flow. The applied magnetic field brings changes in the local

https://doi.org/10.4208/aamm.2014.m600 Published online by Cambridge University Press

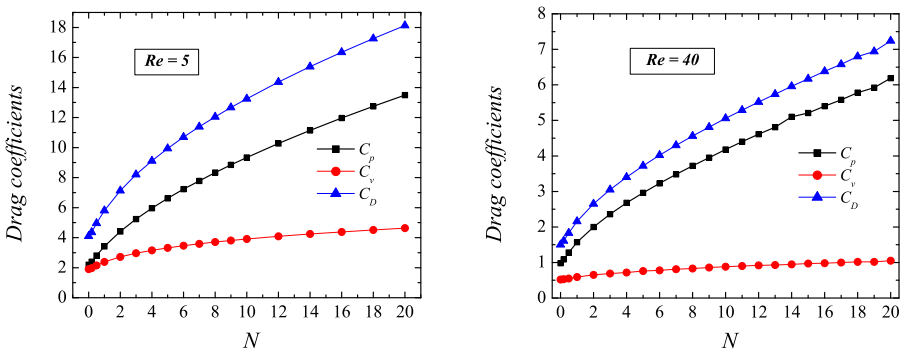


Figure 2: Variation of viscous drag, pressure drag and total drag coefficients as a function of N for $Re=5$ and $Re=40$.

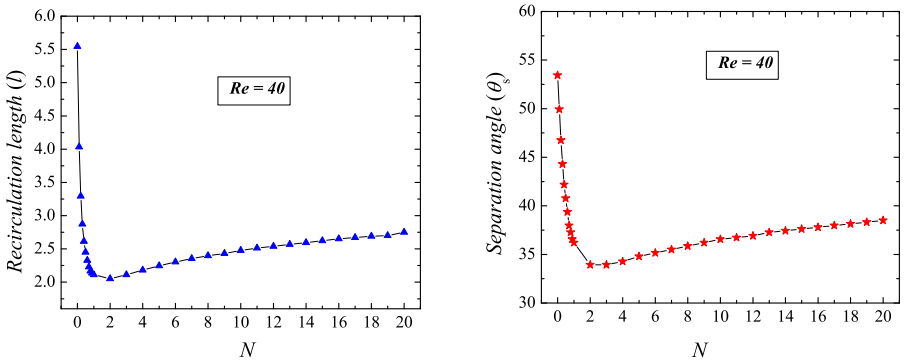


Figure 3: Recirculation length and separation angle as a function of interaction parameter for $Re=40$.

Nusselt number. While studying the dependance of Nu on Pr, when external magnetic field is not present, the maximum heat transfer takes place near the front stagnation point $\theta=\pi$ whereas, when magnetic field is increased, the peak heat transfer region is shifted towards $\theta=\pi/2$. Irrespective of the magnetic field, when Pr is increased, the local Nusselt number increased along the surface of the cylinder. However, the heat transfer rate of a fluid with higher Pr is affected more by external magnetic field when compared to a fluid with lower Pr. Fig. 5 exhibits the dependence of local Nusselt number on various magnetic strengths $N=0$, $N=0.5$, $N=9$ and $N=20$ for $Re=5,40$ and $Pr=0.73,7$. It is clear that higher the Re higher the heat transfer in the case of application of lower magnetic strengths ($N=0,0.2$) as we expected. And the increase of Pr also increases the heat transfer. But when N increases ($N=9$), there is a change in this pattern in the rear stagnation point, that is, the fluid flow for $Re=40$ with $Pr=0.73$ produces less heat transfer when compared with that of for $Re=5$ with $Pr=7$. This implies the influence of Pr is more than the influence of Re in terms of heat transfer at higher magnetic strengths. Figs. 6 and 7 explains about the heat transfer changes along particular radial lines at $\theta=0$, $\pi/6$, $\pi/2$, π with variation of N for different Pr. It is clear that when N increases Nu decreases along

https://doi.org/10.4208/aamm.2014.m600 Published online by Cambridge University Press

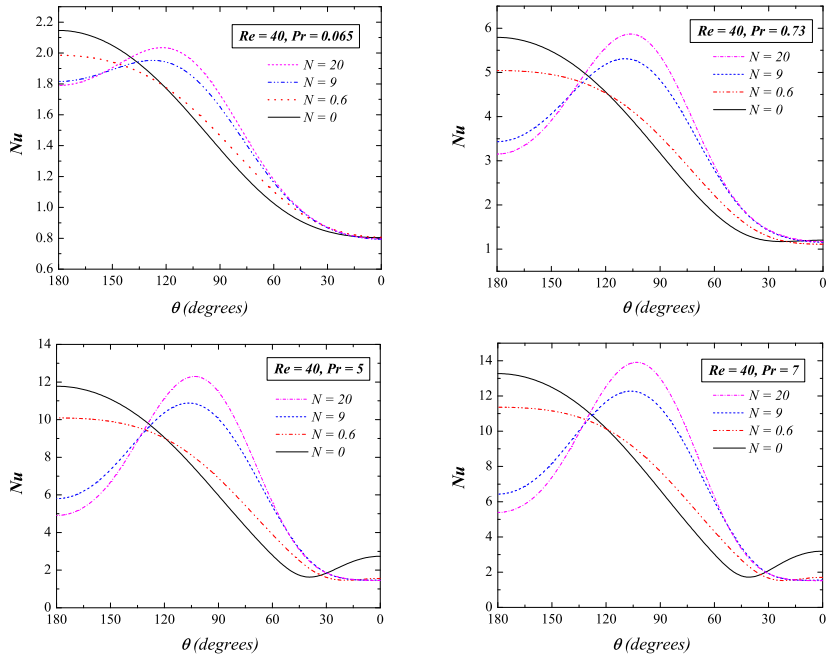


Figure 4: Angular variation of the Nusselt number for $Re=40$ when $Pr=0.065$, 0.73, 5 and 7.

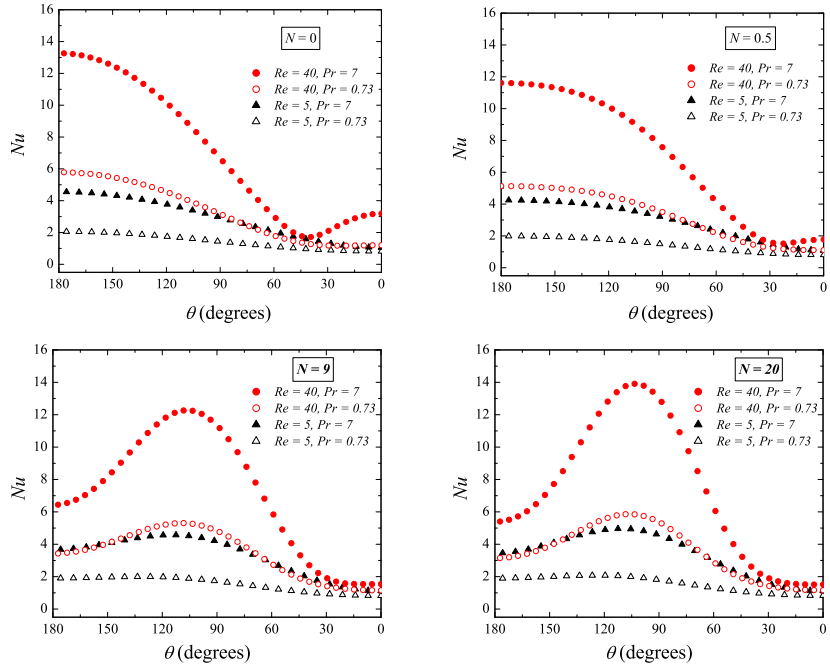


Figure 5: Dependence of local Nusselt number Nu on $N=0$, $N=0.5$, $N=9$ and $N=20$ for different Prandtl numbers with $Re=5$,40.

https://doi.org/10.4208/aamm.2014.m600 Published online by Cambridge University Press

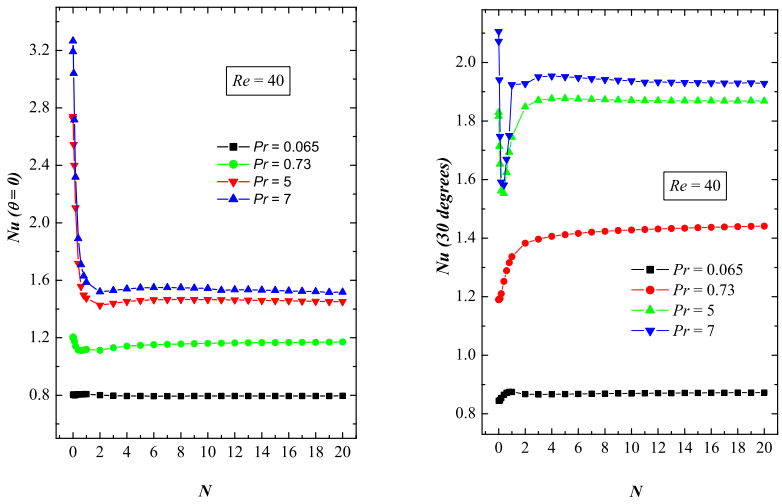


Figure 6: Variation of local Nusselt number (a) $Nu\ (\theta=0)$, (b) $Nu\ (\theta=\pi/6)$ with N for $Re=40$.

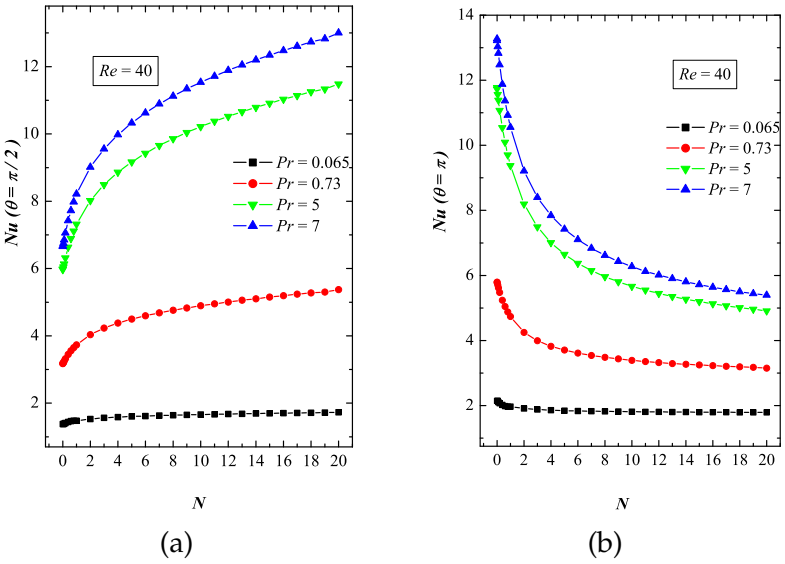


Figure 7: Variation of local Nusselt number (a) $Nu\ (\theta=\pi/2)$), (b) $Nu\ (\theta=\pi)$ with N for $Re=40$.

$\theta=0$ and $\theta=\pi$ whereas a reversal effect is observed when $\theta=\pi/2$. On the other hand the pattern is so different along $\theta=\pi/6$, that is, for $Pr=0.065$, 0.73, Nu increases as N increases. Meanwhile, at higher Prandtl numbers ($Pr=5$ and $Pr=7$) there is a reduction of Nu up to a critical level and then it increases. Hence on applying magnetic field heat transfer is much controlled in the front and rear stagnation points but non-monotonically changes in the region near separation point.

https://doi.org/10.4208/aamm.2014.m600 Published online by Cambridge University Press

4.3 Mean Nusselt number

When these local values of heat flux is surface averaged over the cylinder using Eq. (4.2b), we get mean Nusselt number $\overline{Nu}$. In order to compare with the available results of Uda et al. [3], simulations have been carried over the parameters $Re=5$ and $Re=40$ with $Pr=0.065$ for different N values. In the case of both $Re=5$ and 40 the non-monotonic behavior in the increase/decrease of mean Nusselt number is observed. This fact is in agreement with the observations of Uda et al. [3]. The variation of mean Nusselt number with respect to the magnetic field N for $Re=5$ and 40 in Fig. 8. Here we observe that there is a degradation in mean Nusselt number when $0\leq N\leq 0.2$ for $Re=5$ and when $0\leq N\leq 0.4$ for $Re=40$ beyond which it increases leading to a non-monotonic behavior. This observation is in line with the recent experimental findings of Uda et al. [3] and Yokomine et al. [4]. The magnetic field for which maximum degradation of heat transfer is observed is considered as critical magnetic field. These figures ensure the non-monotonic behavior of $\overline{Nu}$ with respect to Pr too. But the decrease of $\overline{Nu}$ is significantly more in the case of higher Re $(=40)$ than $Re=5$, which says the influence of Re. In Fig. 9, the dependence of

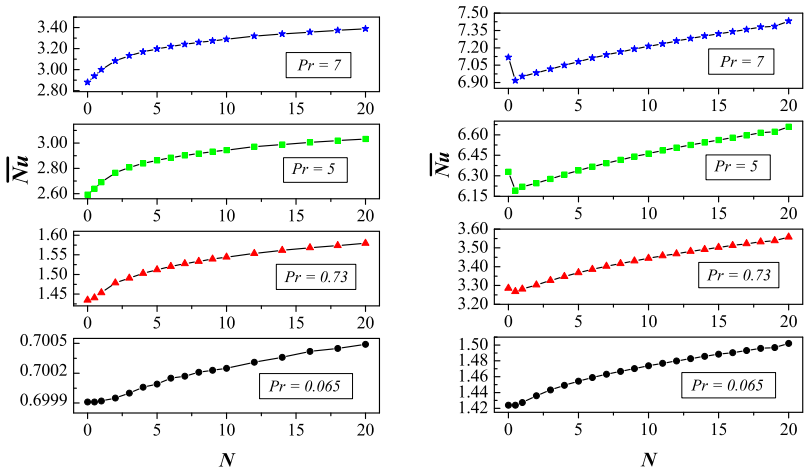


Figure 8: Variation of mean Nusselt number $\overline{Nu}$ with magnetic field N for different Pr for $Re=5$ and 40.

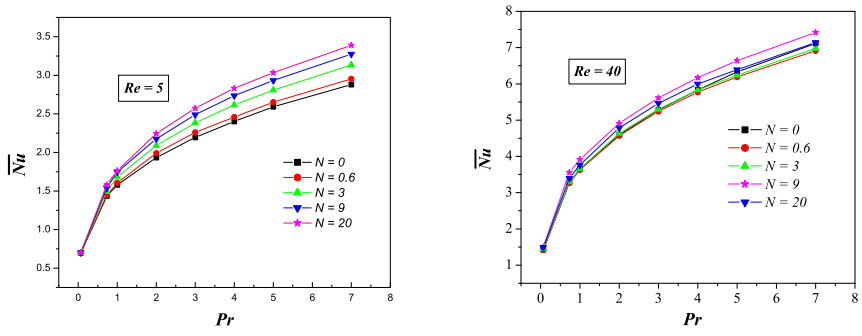


Figure 9: Dependance of mean Nusselt number $\overline{Nu}$ on Pr and N for $Re=5$,40.

https://doi.org/10.4208/aamm.2014.m600 Published online by Cambridge University Press

mean Nusselt number on Prandtl number Pr with variation in the strength of magnetic field N for $Re=5$ and $Re=40$ are presented. An increase of $\overline{Nu}$ with respect to Pr is identified for all N values which matches with the observation (in the absence of magnetic field) made by Kurdyumov and Fernandez [21]. On adding the parameters $Re=10$, 20 with $Pr=0.73$, 5 the comparison on $\overline{Nu}$ is made with available literature in the case when there is no magnetic field applied.

4.4 Temperature field

The role of Re, N and Pr on forced convective heat transfer distribution from isothermal cylinder immersed in magnetohydrodynamic fluid flow are analyzed by means of isothermal contours from Figs. 10 to 12. Due to high thermal gradients (implied by the presence of dense layer of isotherms) near the upstream region close to the surface of the

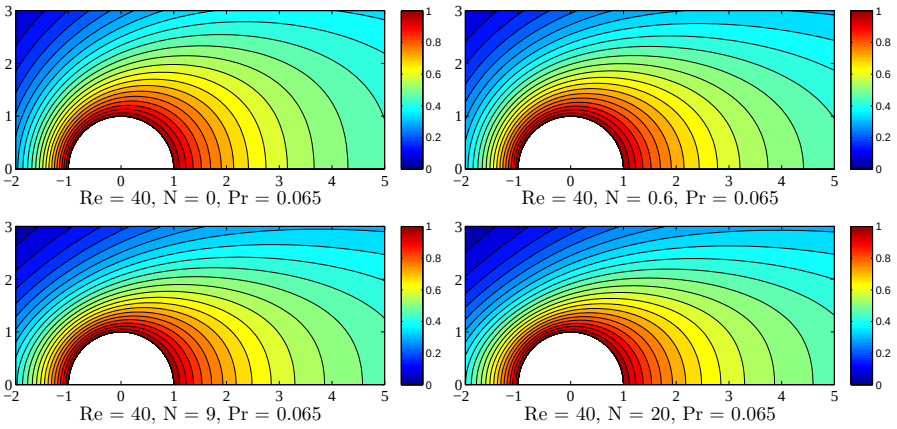


Figure 10: Isotherms of the flow for $Re=40$ with $Pr=0.065$ and $N=0$, 0.6, 9, 20.

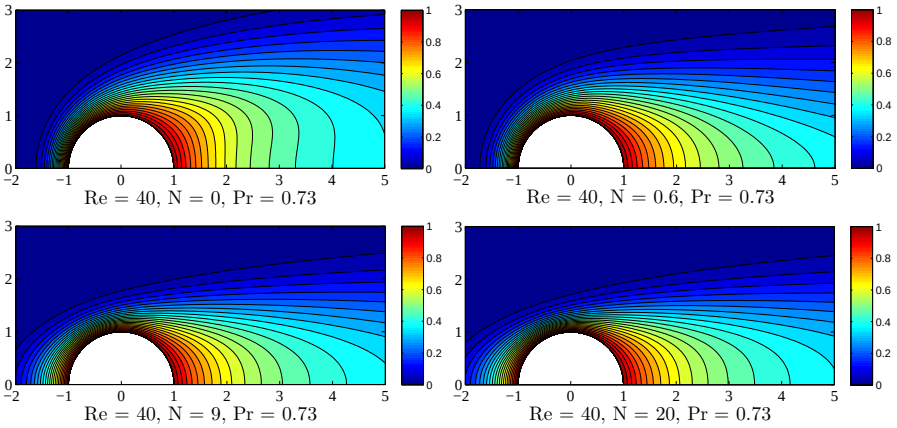


Figure 11: Isotherms of the flow for $Re=40$ with $Pr=0.73$ and $N=0$, 0.6, 9, 20.

https://doi.org/10.4208/aamm.2014.m600 Published online by Cambridge University Press

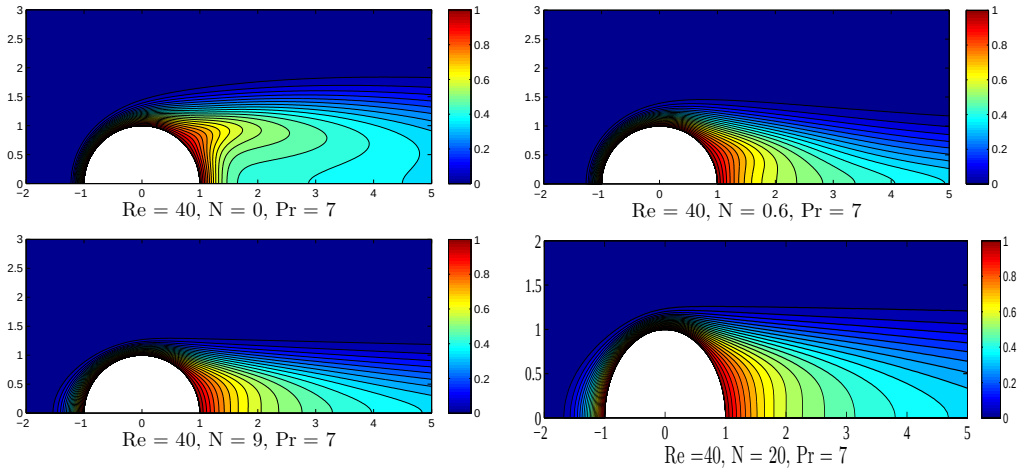


Figure 12: Isotherms of the flow for $Re=40$ with $Pr=7$ and $N=0$, 0.6, 9, 20.

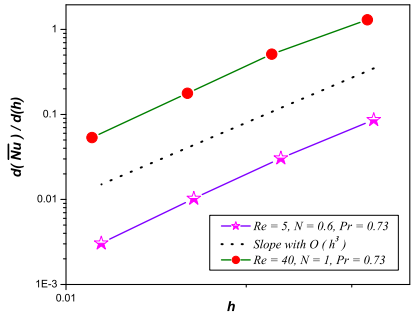


Figure 13: Order of accuracy computed using divided differences of mean Nusselt number obtained from different grids.

cylinder, the local Nusselt number Nu is found to be more and not so in the downstream region. In the absence of magnetic field, as Re increases, there is a shift of higher heat transfer region towards the bluff body surface all along the cylinder. This shift is considerably more at the far down stream region between $0\leq\theta\leq 50$. It is due to the presence of larger recirculation region at higher Re. Further, for the increase of Pr, when $N=0$, isotherms with higher temperature moved towards the surface of the cylinder at the axis of the symmetry whereas it is still away from the cylinder in the region $10\leq\theta\leq 30$. But upon applying magnetic field it uniformly pushed towards the axis of symmetry (Fig. 11). On fixing Pr, for the increase of strength of magnetic field it is observed that the heat transfer is well controlled to move towards the line of symmetry in the down stream region (Fig. 12). A plot of $d(\overline{Nu})/dh$ versus the grid step size is plotted as log-log graph to show the order of accuracy of the numerical solution obtained in this work. The quantity $d(\overline{Nu})/dh$ is calculated using divided difference of $\overline{Nu}$. The slope of the graph is found to be 3 from Fig. 13. Since the quantity plotted on the y-axis contains already

https://doi.org/10.4208/aamm.2014.m600 Published online by Cambridge University Press

one derivative, the actual accuracy of $\overline{Nu}$ is one more than the slope of the plot, which amount to fourth order accuracy, $\mathcal{O}(h^4)$.

5 Conclusions

In this paper, heat transfer from a heated circular cylinder immersed in a steady stream of viscous incompressible and electrically conducting fluid which is under the influence of an applied magnetic field is investigated using higher order finite difference scheme. The non-monotonic behavior of separation length and separation angle is found with the increase of magnetic field. When external magnetic field is not present, the maximum heat transfer takes place near the front stagnation point $\theta=\pi$ whereas, when magnetic field is increased, the peak heat transfer region is shifted towards $\theta=\pi/2$. The heat transfer rate of a fluid with higher Pr is affected more by external magnetic field when compared to a fluid with lower Pr. We observe that there is a degradation in mean Nusselt number up to a critical value of N, beyond which it increases leading to a non-monotonic behavior. This observation is in line with the recent experimental findings.

Acknowledgments

One of the authors T. V. S. Sekhar would like to thank the CSIR for supporting this research work through project grant vide CSIR letter Sanction No. 25(0200)/12/EMR-I.

References

[1] P. A. Davidson, *Magnetohydrodynamics in materials processing,* Annu. Rev. Fluid Mech., 31 (1999), pp. 273–300.
[2] J. H. Boynton, *Experimental study of an ablating sphere with hydromagnetic effect included,* J. Aerosp. Sci., 27 (1960), pp. 306.
[3] N. Uda, A. Miyazawa, S. Inoue, N. Yamaoka, H. Horiike and K. Miyazaki, *Forced convection heat transfer and temperature fluctuations of Lithium under transverse magnetic fields*, J. Nuc. Sci. Tech., 38 (2001), pp. 936–943.
[4] T. Yokomine, J. Takeuchi, H. Nakaharai, S. Satake, T. Kunugi, N. B. Morley, and M. A. Abdou, *Experimental investigation of turbulent heat transfer of high Prandtl number fluid flow under strong magnetic field,* Fusion Sci. Tech., 52 (2007), pp. 625–629.
[5] S. Kenjeres, *Electromagnetic enhancement of turbulent heat transfer,* Phys. Rev. E, 78 (2008), 066309.
[6] W. K. Hussam and G. J. Sheard, *Heat transfer in a high Hartmann number MHD duct flow with a circular cylinder placed near the heated side-wall,* Int. J. Heat Mass Transfer, 67 (2013), pp. 944–954.
[7] D. Chatterjee and K. Chatterjee, *Wall-bounded flow and heat transfer around a circular cylinder at low Reynolds and Hartmann numbers*, Heat Transfer-Asian Research, 42 (2013), pp. 133–150.

https://doi.org/10.4208/aamm.2014.m600 Published online by Cambridge University Press

[8] A. Z. GHADI, H. GOODARZIAN, M. G. BANDPY AND M. S. VALIPOUR, *Numerical investigation of magnetic effect on forced convection around two-dimensional circular cylinder embedded in porous media,* Eng. Appl. Comput. Fluid Mech., 6 (2012), pp. 395–402.
[9] J. LAHJOMRI, P. CAPERAN AND A. ALEMANY, *The cylinder wake in a magnetic field aligned with the velocity,* J. Fluid Mech., 253 (1993), pp. 421–448.
[10] V. SHATROV, G. MUTSCHKE AND G. GERBETH, *Numerical simulation of the two-dimensional MHD-flow around a circular cylinder,* Magnetohydrodynamics, 33 (1997), pp. 5–15.
[11] G. MUTSCHKE, G. GERBETH, V. SHATROV AND A. TOMBOULIDES, *Two- and three dimensional instabilities of the cylinder wake in an external magnetic field*, Phys. Fluids, 9 (1997), pp. 3114–3116.
[12] H. S. YOON, H. H. CHUN, M. Y. HA AND H. G. LEE, *A numerical study on the fluid flow and heat transfer around a circular cylinder in an aligned magnetic field,* Int. J. Heat Mass Trans., 47 (2004), pp. 4075–4087.
[13] Y. V. S. S. SANYASIRAJU AND V. MANJULA, *Flow past an impulsively started circular cylinder using a higher-order semicompact scheme,* Phys. Rev. E, 72 (2005), 016709.
[14] T. V. S. SEKHAR AND B. HEMA SUNDAR RAJU, *An efficient higher order compact scheme to capture heat transfer solutions in spherical geometry,* Comput. Phys. Commun., 183 (2012), pp. 2337–2345.
[15] T. V. S. SEKHAR AND B. HEMA SUNDAR RAJU, *Spherical geometry HOC scheme to capture low pressures within a wake,* East Asian J. Appl. Math., 3 (2013), pp. 93–106.
[16] J. S. BRAMELY, *Magnetohydrodynamic flow past a circular cylinder,* J. Appl. Math. Phys., 25 (1974), pp. 409–416.
[17] J. S. BRAMELY, *Magnetohydrodynamic flow past a circular cylinder-II,* J. Appl. Math. Phys., 26 (1975), pp. 203–209.
[18] T. V. S. SEKHAR, R. SIVAKUMAR AND T. V. R. RAVI KUMAR, *Drag and pressure fields for the MHD flow around a circular cylinder at intermediate Reynolds numbers*, J. Appl. Math., 2005 (2005), pp. 183–203.
[19] G. H. JUNCU, *Conjugate heat/mass transfer from a circular cylinder with an internal heat/ mass source in laminar cross flow at low Reynolds numbers*, Int. J. Heat Mass Transfer, 48 (2005), pp. 419–424.
[20] S. C. R. DENNIS, J. D. HUDSON AND N. SMITH, *Steady laminar forced convection from a circular cylinder at low Reynolds numbers*, Phys. Fluids, 11 (1968), pp. 933–940.
[21] V. N. KURDYUMOV AND E. FERNANDEZ, *Heat transfer from a circular cylinder at low Reynolds numbers,* ASME J. Heat Transfer, 120 (1998), pp. 72–75.

https://doi.org/10.4208/aamm.2014.m600 Published online by Cambridge University Press